



Characterization and antifouling performance of cellulose triacetate forward osmosis membranes modified with graphene oxide

Fang Li^{a,b}, Meilei Sun^a, Qianxun Cheng^a, Qing Tian^{a,*}, Chunyan Ma^a, Manghong Huang^a

^aSchool of Environmental Science and Engineering, Donghua University, Shanghai 201620, China, Tel. 86-21-67792557; Fax: 86-21-67792544; email: tq2004@dhu.edu.cn

^bTextile pollution controlling Engineering center of Ministry of Environmental Protection, Shanghai 201620, China

Received 23 April 2016; Accepted 2 June 2016

ABSTRACT

Forward osmosis (FO) is an emerging membrane separation technology in environmental and industrial process. The prepared membranes with various graphene oxide (GO) nanosheets loading were characterized by morphology and chemical analysis as well as model fouling tests in this paper. The result showed that the addition of GO nanosheets in casting solution led to an improvement in hydrophilicity, porosity, stress tensile and water permeability for the modified cellulose triacetate (CTA) membrane. As for the model fouling tests, the GO-modified CTA membrane presented an advantage of antifouling ability to biopolymers and oil emulsion. It was also found that the increase of ionic strength caused by reverse salt leakage affects the bovine serum albumin (BSA) fouling more significantly than sodium alginate (SA) fouling due to charge screening reduces the electrostatic repulsion between BSA molecules and membrane surface. The GO-modified membranes presented an ideal performance in oil emulsion separation due to its high hydrophilicity.

Keywords: Forward osmosis; Graphene oxide; Antifouling; Biopolymer; Oil

1. Introduction

As problems with water scarcity occurred globally in the last decades, a shortage of fresh water is one of the acute challenges facing the world today [1]. Pressure-driven membrane processes including microfiltration (MF), ultrafiltration (UF), nanofiltration (NF), and reverse osmosis (RO) have been widely used for water treatment and desalination to solve the scarcity of fresh water. However, the main problems arising upon the operation of the membrane units were the membrane fouling, high energy cost, and chemical washing. To date, forward osmosis (FO) technology has displayed great potential in a wide variety of applications as it is driven by the difference of osmotic pressure between a draw solution (DS) and a feed solution (FS) through a semi-permeable membrane [2]. Compared with traditional pressure-based membrane processes, FO offers many advantages which consist of lower energy and operational cost, negligible

hydraulic pressure and decreased fouling tendency [3]. However, the performance on water flux, solute rejection, mechanical strength, and chemical stability has limited the practical application of FO process [4].

The major bottleneck of FO is the severe internal concentration polarization (ICP) in the porous membrane support [5]. ICP is caused by a net osmotic pressure difference across the membrane, as the actual net osmotic pressure is remarkably less than the theoretical osmotic pressure [6]. Currently used membranes for FO include thin-film composite (TFC) membrane made of polymerization on a polysulfone layer supported by non-woven fabrics [7], asymmetric membranes made of CTA coated on polyester mesh [8], and hollow fiber membranes developed recently [9]. These membranes have a non-selective and low-porosity support layer rendering them suffer from severe ICP which greatly reduces the effective driving force. Thus, an ideal support layer for an FO membrane should be highly porous, low tortuous, and thin in structure [10], resulting in desirable water flux and minimized ICP for FO process [11,12].

* Corresponding author.

Graphene oxide (GO) currently has attracted considerable interest in membrane material investigation due to its intrinsic properties [13]. Although the structure of GO is difficult to be described accurately, most researchers accept that the model of GO sheet distributes the hydroxyl and epoxy groups at random [14]. These polar functional groups can act as antifouling factors enhancing the hydrophilicity of the GO-polymer mixed membranes [15–17]. PVDF-GO composite UF membranes prepared by Zhang et al. using phase inversion method had larger mean pore size and water flux [18]. Ionita et al. found that the flux of the PSf/GO loose composite membranes via phase inversion method decreased with GO addition, and it was assigned to the stabilization of composite membrane structure [19]. Hegab et al. attached GO nanosheets to the polyamide selective layer of TFC FO membranes through a poly-L-Lysine intermediary using either layer-by-layer or hybrid grafting strategies and found that the modified membrane was reflected in reduced flux decline compared with all other samples when filtering brackish water under biofouling conditions [20]. Chung et al. improved the performance of GO-embedded nanocomposite hollow fiber membranes by introducing 1-methylnicotinamide chloride to improve the interfacial interactions between the GO nanosheets and the sulfonated polyphenylenesulfone polymer, and observed substantial reductions in reversible, irreversible, and adsorption-induced resistances as well as flux drop [21].

In this work, the CTA FO membranes were modified by incorporating GO nanosheets in CTA matrix with phase inversion method. The modification was expected to optimize the structure of FO membrane, mitigate the ICP effect, and enhance the antifouling ability. The antifouling property of the modified CTA membrane was studied through the evaluation of flux decline during the separation of model foulant solution containing biopolymers or oil.

2. Material and method

2.1. Materials

CTA (43–49 wt.% acetyl) was provided by Celanese Co, Ltd. (USA). Polymers were dried in 80°C vacuum oven prior to using 1,4-dioxane (99.5%), acetone (99.5%), acetic acid (99.5%), ether, hexane, and H₂O₂ (30%) were purchased from Aladdin Co. Ltd, China. Bovine serum albumin (BSA, Aladdin), sodium alginate (SA, Aladdin), and sodium chloride (99.5%, Aladdin) were employed to prepare FS and DS. Graphite powders were produced by the Qingdao Ruisheng Graphite Co., Ltd. (China) to be used for the exploration of membrane fouling. The vegetable and mineral oil were purchased from the supermarket named Dalunfa.

2.2. Preparation of GO

GO was prepared by improved Hummers' method, as described elsewhere [22]. In brief, a 9:1 mixture of concentrated H₂SO₄/H₃PO₄ (360:40 mL) was added to a mixture of graphite flakes (3.0 g) and KMnO₄ (18.0 g), producing a slight exotherm to 35–40°C. The reaction was then heated to 50°C and stirred for 12 h. The reaction was cooled to room temperature and poured onto ice (400 mL) with 30% H₂O₂ (3 mL).

The filtrate was centrifuged (4,000 rpm for 4 h), and the remaining solid material was then washed in succession with 200 mL of water, 200 mL of 30% HCl and 200 mL of ethanol. The material remaining after this extended, multiple-wash process was coagulated with 200 mL of ether, and the resulting suspension was filtered over a 0.45 µm PVDF membrane. The solid obtained on the filter was vacuum-dried overnight under ambient air, obtaining 5.8 g of product.

2.3. Membrane fabrication

CTA flat-sheet membrane was prepared by immersed phase-inversion process [6]. In this study, the composition of casting solutions used in this study is shown in Table 1. It was clear that three GO modified membranes were fabricated with various GO weight loading about 0.5%, 1% and 2% in dry membranes. At first, CTA was dissolved in the solvent of 1,4-dioxane under magnetic stirring for 5 h at 85°C. Then, acetic acid, acetone and GO were added in the blend solution under continuous stirring at 200 rpm for 3 h at 40°C until the solution became completely homogenous. To complete the dispersion of GO nanosheets in the casting solution, the solution was exposed to ultrasonic wave for 1 h. Next, the homogeneous solution was then cast on a clean glass plate evenly using a casting knife with a thickness of 150 µm. The casted film was immersed in the tap water coagulant bath with a temperature of 5°C for phase separation after partial evaporation of the solvent for 60 s. Finally, the as-cast membrane was gently peeled off from the glass plate and then soaked in deionized water (DI) at room temperature overnight to remove the residual solvent. The membranes were annealed at 85°C for 15 min in water before using.

2.4. Membrane characterization

The membrane morphology was examined by scanning electron microscopy (SEM, JSM-5600LV, Japan). The atomic force microscopy (AFM) measurements were performed on a Multimode AFM with Nanoscope IV Multi Mode Controller (Veeco, USA) using the software supplied by the manufacturer. To characterize the functionalized polymers and membrane surfaces, by using the ATR-FTIR spectroscopy (Bruker, Tensor27, German), the contact angle (CA) measurements were performed using a CA goniometer (SL-200c, Solon Technology science Co., Ltd. Shanghai). The data are reported as the average values and standard deviations of six measurements. Mechanical strengths were measured by Adv. Mater.

Table 1
Composition and concentration of casting solutions for modified CTA membranes

Membrane	CTA (wt.%)	Acetone (wt.%)	Acetic acid (wt.%)	1,4-dioxane (wt.%)	GO (wt.%)
CTA	10	15	5	70	0
CTA-0.5%GO				69.95	0.05
CTA-1%GO				69.9	0.1
CTA-2%GO				69.8	0.2

Testing System (H5KS-1105, Hounsfield Ltd., UK), using membrane samples with 100 cm × 1 cm dimensions. The thickness of the membrane sample was determined by a digital micrometer. Five measurements were performed at a cross-head speed of 2 mm·min⁻¹, and the values were averaged.

For the measurement of the substrate membrane porosity ϵ (%), Eq. (1) was employed by taking into account the change in membrane weight before and after drying:

$$\epsilon = (W_1 - W_2) / A_m \delta \rho \tag{1}$$

where, W_1 and W_2 are the weight of wet membrane and dry membrane, respectively. A_m and δ are the effective membrane area and thickness, respectively, and ρ is water density.

2.5. Evaluation of the membrane performance

A laboratory-scale, cross-flow RO unit was utilized to determine the water permeability A and salt permeability coefficient B , as shown in Fig. 1. The water permeability coefficient of the FO membranes, A , was acquired with the Eq. (1):

$$J = \frac{\Delta V}{A_m \Delta t} \tag{2}$$

$$A = \frac{J}{\Delta P} \tag{3}$$

where J , A , A_m , ΔV , Δt and ΔP are water flux, water permeability, the effective membrane area, the permeate volume, time and cross membrane pressure, respectively.

DI water was used as feed during the acquisition of A . Subsequently, the salt rejection, R , was determined from the measured conductivities of permeate and feed by using feed water containing 2,000 ppm NaCl at 5 bar with a cross-flow velocity of 0.25 m·s⁻¹. The flux was recorded for 1 h to calculate the A coefficient.

$$R = (1 - \frac{C_p}{C_f}) \times 100\% \tag{4}$$

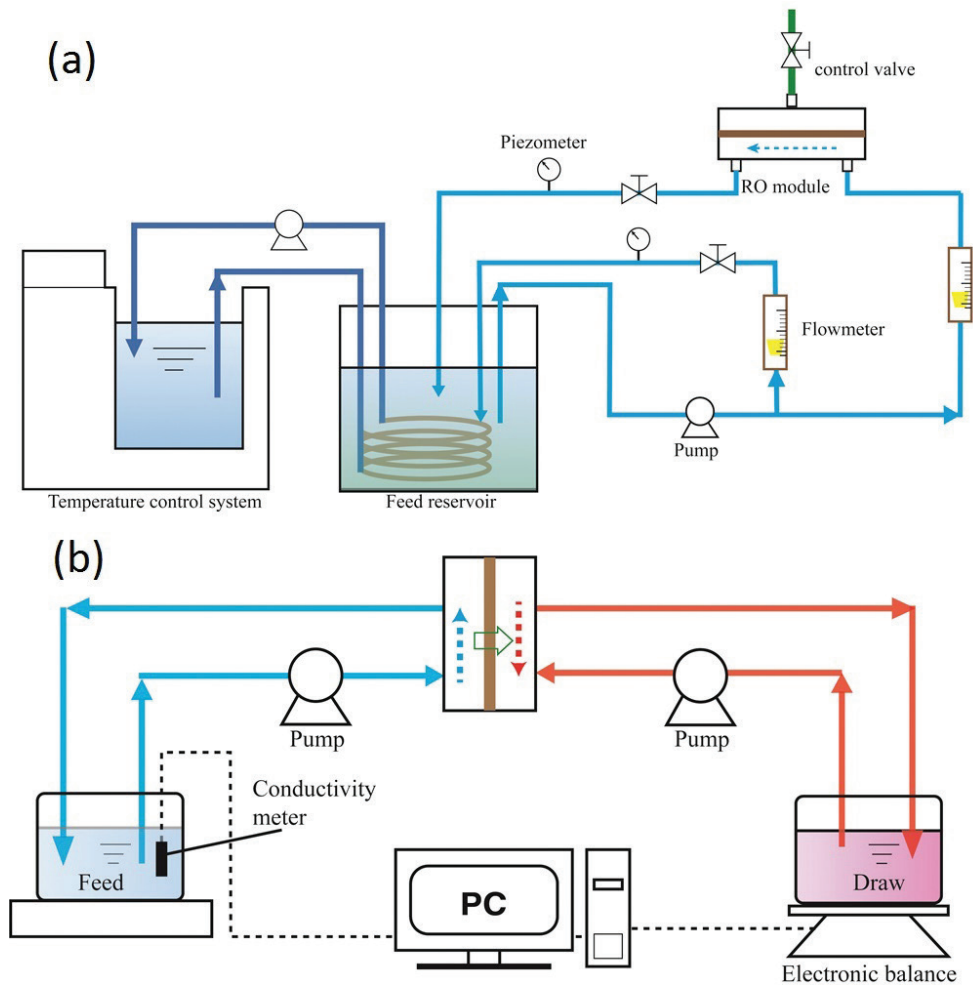


Fig. 1. Schematic diagram of laboratory-scale: (a) cross flow reverse osmosis, (b) forward osmosis (FO) system for membrane separation performance.

where C_p and C_f are the salt concentrations of permeate and FS, respectively. The salt permeability coefficient, B , an intrinsic property of membrane skin layer, was calculated based on the solution-diffusion theory [20].

$$B = \left(\frac{1}{R} - 1\right) \times J \quad (5)$$

The FO membranes performance, including water flux and reverse salt flux, was evaluated with a laboratory-scale FO setup as described in other literatures. As shown in Fig. 1, a cross-flow membrane filtration cell unit with an effective filtration area of 40 cm² was applied to test control and modified membranes, similar to previous investigations. This membrane module contained channels on both sides of the membrane for FS and DS, respectively. The effective dimensions of each channel were measured as 10 cm (length), 4 cm (width) and 0.2 mm (height). The temperature of the FS and DS were maintained at 25 ± 1°C. DI water and 1.0 M NaCl solution were used as the FS and raw solution, respectively. The experimental water flux J_v was calculated by measuring the change in the feed container mass with time by Eq. (6) [23]:

$$J_v = \frac{\Delta V}{A_m \times \Delta t} = \frac{\Delta m / \rho}{A_m \times \Delta t} \quad (6)$$

where A_m is the effective membrane surface area, Δt is the measuring time interval, ρ is the water density and Δm is the measured weight interval for the water that permeated from the FS to the DS. The reverse salt flux J_s of the DS was calculated as:

$$J_s = \frac{\Delta(C_i V_i)}{A_m \times \Delta t} \quad (7)$$

where C_i and V_i are the concentration and volume of FS at the end of each test, respectively. As for FO membrane, the structure parameter is one of the essential properties. In addition to this, the classical ICP model is also determining membrane structural parameter S , as the following equation [24, 25]:

$$J_v = \frac{D}{S} \left[\ln \frac{A\pi_{draw} - J_v + B}{A\pi_{feed} + B} \right] \quad (8)$$

$$J_v = \frac{D}{S} \left[\ln \frac{A\pi_{draw} + B}{A\pi_{feed} + J_v + B} \right] \quad (9)$$

where D is the salt diffusion coefficient; π_{draw} and π_{feed} are the osmotic pressures of the DS and FS, respectively.

The parameter S is one of the critical properties of FO membranes, defined as the membrane thickness δ and tortuosity τ over its porosity ε [20]:

$$S = \frac{\delta\tau}{\varepsilon} \quad (10)$$

2.6. Antifouling tests

To explore the antifouling ability of the modified membrane, the model foulants including BSA, SA and oil were used in this work. These different kinds of oil to represent oil foulants are elaborated as follows. Hexane (n-hexane, C₆H₁₄) is the alkane that is in stable liquid form at room temperature with the smallest carbon number in molecule. Mineral oil is a mixture of hydrocarbons with 15–40 carbon atoms in one molecule, which is a commercially available pump lubricating oil produced by Sinopec, China. The vegetable oil used in this work is sunflower oil (Luhua, China). The oil 30 g·L⁻¹ emulsion of oil/Tween-80 in water (9:1 ratio of oil to surfactant) was prepared by blending with a blender at 20,000 rpm for 3 min. The emulsion was then cooled to 25°C and diluted into 15,000 mg·L⁻¹ model solution in the FO test system feed tank. The model solution of BSA and SA was prepared with a 200 mg·L⁻¹ concentration. The protocol of fouling test in this work was described as follows. First, a control experiment for baseline was conducted with a FS of DI water to measure the extent of flux decline exclusively due to DS dilution and solute reverse diffusion. Then, the fouling experiment was conducted (with model foulant solution as feed) at the same initial flux as the control experiment. In this case, the flux decline caused by the combined effect of DS dilution, solute reverse diffusion, and membrane organic fouling was observed.

3. Results and discussion

3.1. Characterization of GO nanosheets

The ATR-FTIR spectra and X-ray diffraction (XRD) patterns of GO were present in Fig. 2. The peaks at 3,424 cm⁻¹ and 1,397 cm⁻¹ of the GO nanosheets in FTIR spectra were assigned to O-H stretching and O-H deformation, respectively. The C=O stretching vibration in the carboxyl group of GO was obviously visible around 1,726 cm⁻¹, whereas the peak at 1,088 cm⁻¹ was due to the C-C stretching of epoxy and alkoxy groups [26]. The peak at 1,630 cm⁻¹ was assigned to the vibrations of the adsorbed water molecules and the contributions from the vibration of aromatic C=C [27]. As for the XRD patterns, the strong peak centered at around 10.7° and the other peak at about 22° correspond to the characteristic reflection of GO and (002) interplanar spacing [28].

3.2. Characterization of modified CTA membranes

Fig. 3 shows the SEM images of the top surface, cross-section and bottom surface of unmodified and modified CTA membranes. It was evident that all CTA membranes prepared by phase inversion had the asymmetric structure with dense top surface, porous bottom surface and sub-layer with finger-like macrovoid. The dense top surface may be attributed to rapid acetone evaporation during the cast and subsequent solvent outflow to the surrounding water when immersing the nascent membrane into the coagulation bath. Clearly, the surface morphology of modified membrane changed gradually with GO loading. From the SEM images of top surface, both of quantity and size of the dark concaves increased with the GO loading. It was speculated that the high GO loading possibly resulted in

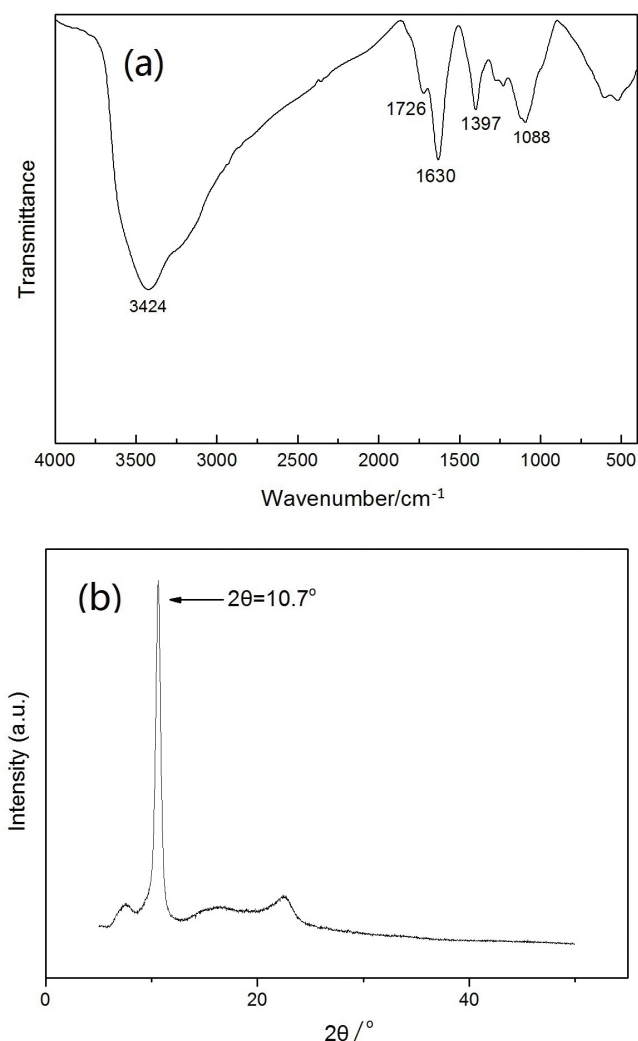


Fig. 2. Characterization of GO nanosheets: (a) FTIR spectra and (b) powder XRD patterns.

the presence of aggregated GO clusters as shown in Fig. 3. Similar tendency was obtained on the bottom surface that the pores were getting more significant with the higher GO loading. The porous membrane surface of CTA-GO membranes might result in a reduction in separation. Furthermore, the contaminants in feed water may enter the membrane body causing unrecoverable fouling. Meanwhile, the finger-like macrovoids in cross-section distributed more regularly with higher GO loading. It can be explained by the fact that GO nanosheet are hydrophilic in nature, and exhibit high affinity toward water. During the phase inversion processes, the high counter diffusion velocity of solvent and non-solvent contributes to the high porosity and pore size in membranes [29]. Thus, instantaneous demixing often results in the formation of macrovoids in membrane structure, whereas slow demixing leads to denser structures [30]. The presence of GO nanosheets as a hydrophilic additive increased the thermodynamic instability of the cast film and led to instantaneous demixing during phase inversion. On the other hand, due to the excellent dispersion of GO nanosheets in casting solution, the finger-like macrovoids were formed with more uniform

distribution [31]. Yet, the agglomeration of GO was more severe when the GO content in casting solution increased. Hence, more agglomerated GO clusters exposed on the top surface. Consequently, addition of GO nanosheets in casting solution led the modified membrane to be more permeable and hydrophilic to some extent.

In addition, tiny filaments were observed on the macrovoid surface for the CTA-GO membranes as shown in Fig. 3 which were absent for CTA membranes. These filaments were supposed to be formed due to the increase of casting solution viscosity which maybe was induced by a slight interaction between GO nanosheet and CTA molecule [32]. However, the change in the viscosity of the casting solution cannot be detected with a common viscometer due to its limited sensitivity.

Membrane surface roughness plays an important role in membrane antifouling performance. A greater membrane roughness increases the total surface area to which foulants can be attached, and the ridge-valley structure favors the accumulation of foulants at the surface [33]. As shown in Fig. 4 and Table 2, it can be found that the roughness of membrane was decreased with the GO loading. During the phase inversion, the hydrophilic nanosheets might act as barriers against the movement of non-solvent. In other words, solvent molecules can diffuse more readily and rapidly from polymer structure while the polymers dragged by GO nanosheets remained stable relatively. Consequently, the smoother membrane surface was formed with the higher GO loading in the casting solution.

As it is well known, CA measurement is the common evaluation approach for hydrophilic/hydrophobic properties of membrane. It was clear that the CA of GO-modified membranes decreased with the GO loading. As shown in Fig. 5(a), the CA of CTA membrane was about 63°, while the average value of CTA-2%GO membrane decreased to 20.6°. As mentioned above, numerous GO nanosheets and clusters exposed on the dense top surface during the cast. The semi-buried GO nanosheets and clusters effectively enhanced the surface wettability due to the high hydrophilicity of functional groups on GO. Moreover, the changes in morphology induced by GO also led to a decrease of CA value of the modified membrane [34].

As shown by the FTIR spectra in Fig. 5(b), characteristic peaks were observed at 1,720; 1,369; and 1,221 cm⁻¹, which were associated with the stretching vibration of C=O, C-CH₂, and C-O-C, respectively [35]. The spectrum of GO modified membrane appeared weak peaks at 3,430 and 2,939 cm⁻¹ associated with the stretching vibration of the O-H and C-H band which were more significant with higher GO loading [15]. Accordingly, the existence of GO nanosheets on the membrane surface was confirmed.

As revealed by XRD analysis in Fig. 5(c), the XRD patterns for the CTA membrane displayed peaks at 2θ = 22.3° which are typical of neat CTA [36]. The modified membranes exhibited peak at 2θ = 13.58° which was absent in pure CTA membrane. As for the little shift of peak locations, it revealed that the GO nanoparticles have been distributed to the membrane matrix, and there may also be existed a slight interaction between GO nanosheet and CTA molecule [32].

The profile of tensile stress and the corresponding data of the pure and GO-modified CTA membranes as a function of GO loading at room temperature are shown in Fig. 5(d)

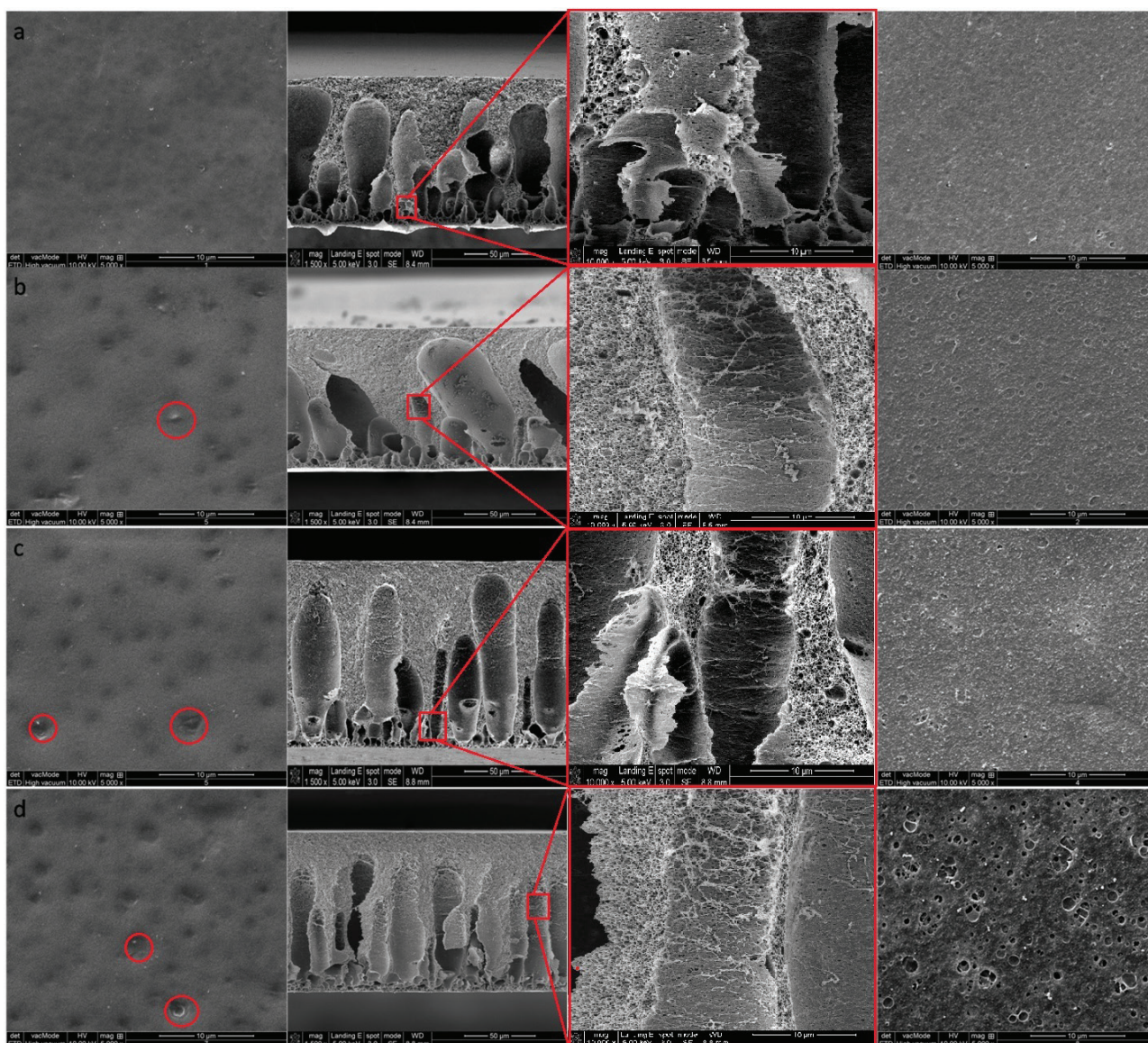


Fig. 3. (a) CTA membrane, (b) CTA-0.5%GO membrane, (c) CTA-1%GO membrane, (d) CTA-2%GO membrane (right image for membrane surface, middle two images with magnification times of 1,500 and 10,000 for cross section, left image for membrane bottom).

and Table 3. Evidently, GO incorporation in CTA matrix was useful to improve the tensile strength and modulus of elasticity of the membrane samples. The tensile strength of the CTA membrane increased from 104 to 128 MP after the CTA incorporated with 2%GO nanosheets. The elastic module of CTA-2%GO membrane was approximately two times higher than that of pure CTA membrane (from 2.4 to 4.6 MPa). It certainly demonstrated that the hydrogen-bonding between $-\text{COOH}$ groups in the GO and $-\text{C}=\text{O}$ groups in the CTA molecules was formed at the interfaces in the CTA matrix, which led to the enhancement of the tensile strength and Young's modulus of GO-modified membranes [37].

3.3. Properties of modified CTA membranes

The separation properties of CTA membrane including salt rejection, water permeability A , and salt permeability B

were summarized in Table 4. The result of the porosity measurement was consistent with the observation based on SEM analysis that the porosity increased with the GO loading. The presence of the GO nanosheets was able to limit the molecular motions of the CTA polymer chains resulting in an increase in the mean distance (free volume) between the polymer chains. Limited molecular motions and increasing mean distance between chains contributed to a simultaneous improvement of membrane porosity [38]. With respect to water permeability, the performance of GO-modified CTA membranes was better than the pure CTA membranes. The improvement of water permeability can be ascribed to the increasing of hydrophilicity and porosity of membrane structure as the A values increased with the increasing of GO lading. It was surprising that the A value of the CTA-2%GO increased sharply to $4.07 \text{ LMH}\cdot\text{bar}^{-1}$, almost two times more than the water permeability of CTA-1%GO with $1.93 \text{ LMH}\cdot\text{bar}^{-1}$. In contrast,

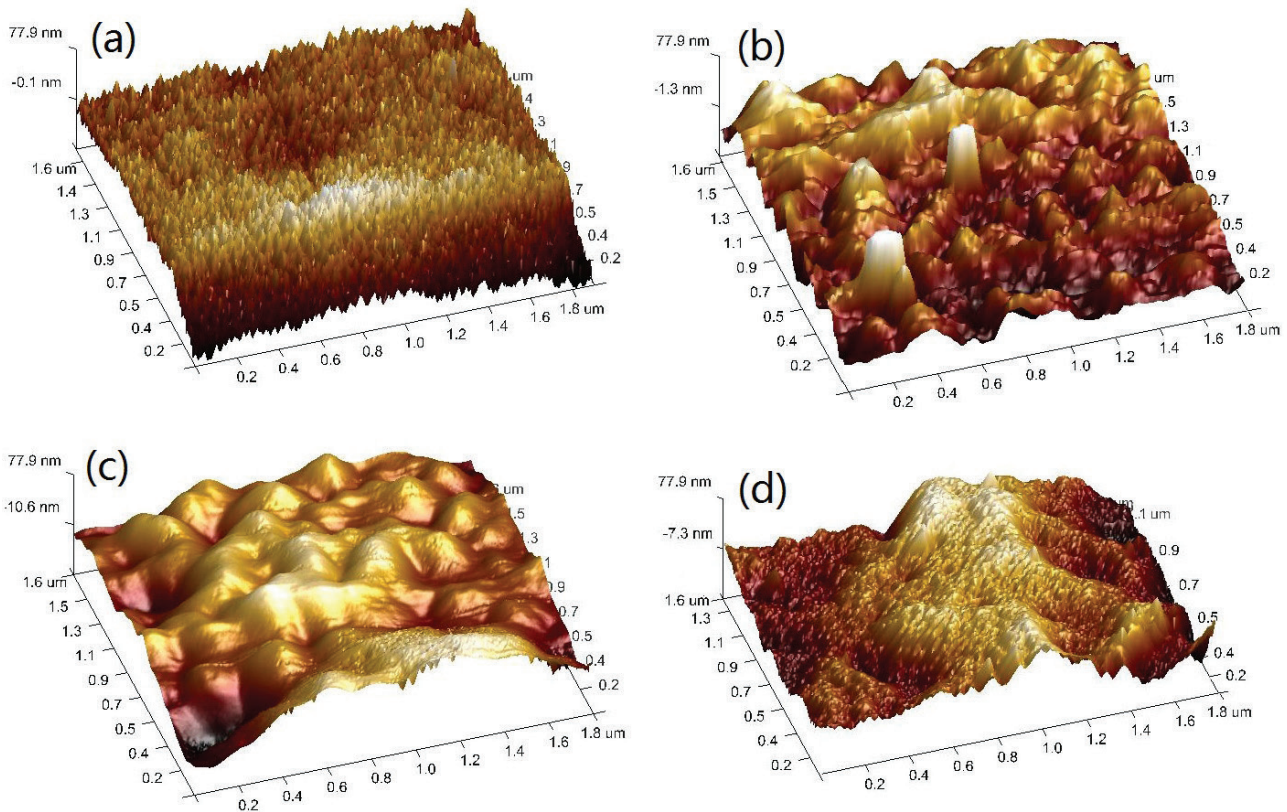


Fig. 4. AFM of membranes: (a) CTA membrane, (b) CTA-0.5%GO membrane, (c) CTA-1%GO membrane, (d) CTA-2%GO membrane.

Table 2
Surface roughness parameters of the membranes by AFM analysis

Membrane	R_a^* (nm)	R_q (nm)	R_z (nm)
CTA	45.9	55.6	168.7
CTA-0.5%GO	15.9	20.3	60.5
CTA-1%GO	14.5	18.9	71.9
CTA-2%GO	9.42	12.8	108.9

* R_a is the arithmetic average of the absolute values of the surface height deviations measured from the mean plane; R_q is the root mean square average of height deviations taken from the mean data plane; and R_z is maximum vertical distance between the highest and lowest data points in the image.

the salt rejection of modified membrane declined with the increase of water permeability. The CTA membrane exhibited the lowest salt permeability (about $11.87 \times 10^{-8} \text{m} \cdot \text{s}^{-1}$) while the CTA-2%GO membrane had the highest salt permeability. For the unusual water and salt permeability of CTA-2%GO membrane, it was supposed that the defects, that is, large pores, were formed on the membrane surface caused by GO agglomeration at high loading. The increase of water and solute permeability are consistent with the GO loading of dense layer, which decreased the resistance against both water and solute transport. In addition, the solute permeability/the water permeability B/A ratio increased as the GO loading increased. The B/A ratio is an important selectivity parameter in FO applications, and it is related directly to the solute reverse

transport [39, 40]. A larger B/A ratio, which means a lower selectivity, is likely to cause more severe solute reverse diffusion from the DS into the feed water and lead to undesirable solute accumulation in FO systems. It also agreed with the S values of 0.87 mm for CTA membrane decreased to 0.57 mm for CTA-1%GO membrane. In common, the lower the S value, the less severe the ICP [41]. In this work, the GO-modified membranes presented smaller B/A ratio and S value, indicating the superior separation properties.

The water flux (J_w) and reverse salt flux (J_s) of the CTA and GO-modified membranes in both membrane orientations with DI water and 1.0 M NaCl solution used as the FS and DS were illustrated in Fig. 6. The result showed that the water flux of GO-modified membrane increased with the GO loading was in consistence with that of RO test. However, the enhancement of reverse salt leak was more significant than that of water flux. Generally, there is a strong trade-off between water permeability and selectivity in FO membrane process. Although the improvement of surface hydrophilicity and sub-layer porosity could result in an increasing of water permeability to a certain extent, the defects on surface were supposed to be the major contributor for the high water flux. The main reason could be that larger and more aggregated clusters of GO emerged on the membrane surface as the content of GO nanosheet in the casting solution increased. As it suffered less dilutive ICP which reduced the osmotic pressure gradient within the support layer in AL-DS mode, the higher flux values of all membranes were obtained operated under this mode. Meanwhile, higher concentration differences across the membrane resulted in the higher J_s values obtained under AL-DS mode [42].

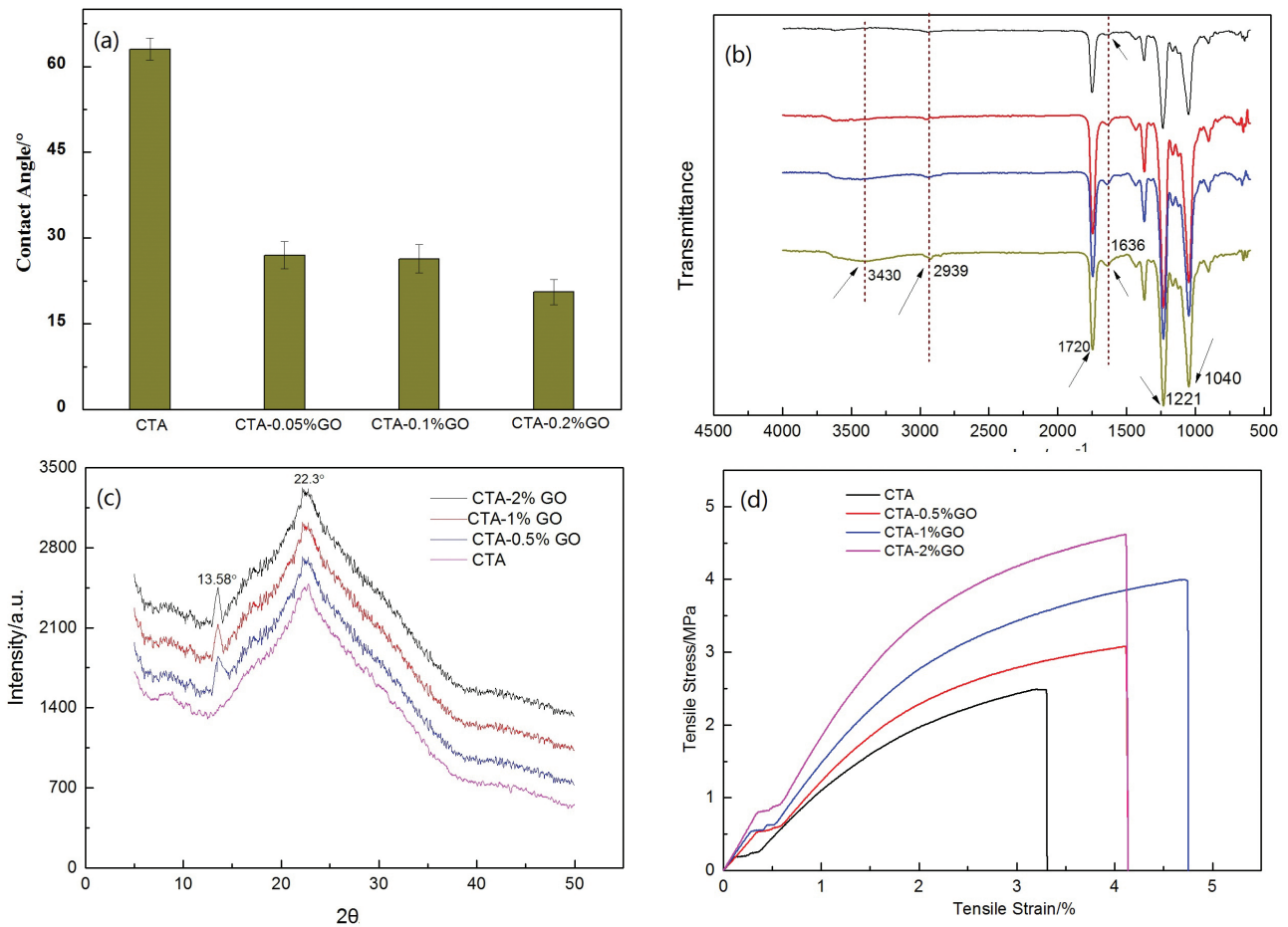


Fig. 5. (a) ATP-FTIR spectra, (b) contact angles, (c) XRD patterns, (d) stress-strain curves of the membranes.

Table 3
Tensile modulus and tensile strength of different membranes

Membrane	Tensile modulus (MPa)	Tensile strength (MPa)
CTA	104 ± 6	2.40 ± 0.05
CTA-0.5%GO	110 ± 5	3.05 ± 0.02
CTA-1%GO	122 ± 8	4.02 ± 0.10
CTA-2%GO	128 ± 10	4.60 ± 0.17

Table 4
Transport properties of CTA and modified membranes based on RO and FO tests

Membrane	Porosity (%)	A (LMH·bar ⁻¹)	B (10 ⁻⁸ m·s ⁻¹)	B/A (kPa)	Rejection (%)	S (mm)
CTA	43.8	1.39	11.87	30.67	87.61	0.87
CTA-0.5%GO	46.3	1.56	29.45	67.98	79.26	0.85
CTA-1%GO	51.2	1.93	93.45	174.17	59.30	0.57
CTA-2%GO	53.1	4.07	206.75	182.71	53.23	0.67

3.4. Antifouling performance of modified membranes

For the purpose of studying GO-modified membrane antifouling ability to biopolymers, like proteins and polysaccharide [43], BSA and SA were used to simulate the model foulants under AL-FS mode. It can be found that the water flux for all membranes with BSA and SA solution as FS in Fig. 7 was lower than that with DI water in Fig. 6. Under the AL-FS mode, the water flux of the CTA membrane can reach 11.1 LMH with the DI water as FS, while initial water flux reduced to 7.6 LMH for SA solution and 8.5 LMH for BSA solution. However, the initial water flux of GO-modified membrane decreased slightly during the separation of the model foulant solution comparing to the DI water. In the case of CTA-0.5%GO membrane during SA solution separation, the flux remained at 10.8 LMH,

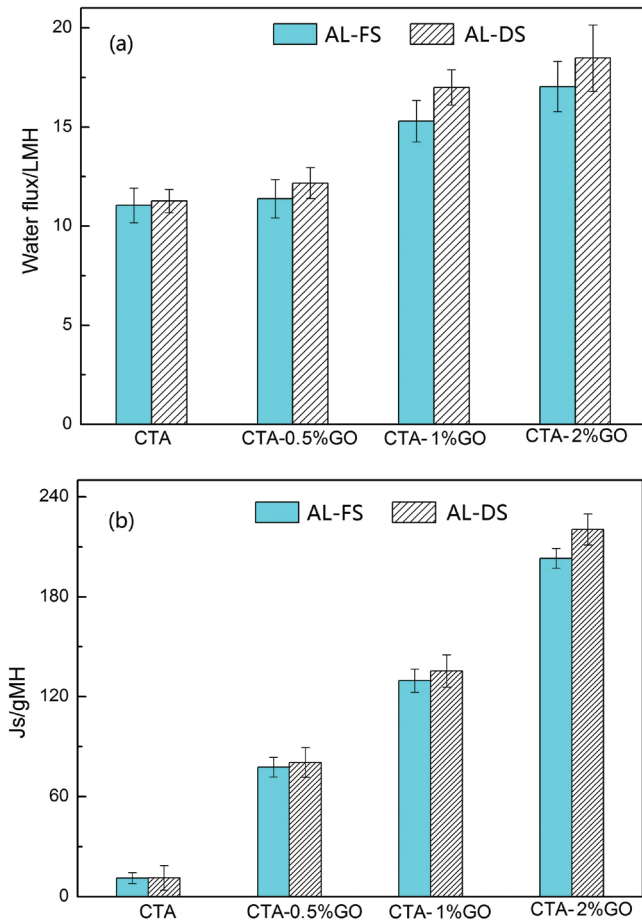


Fig. 6. (a) Water permeation flux, J_v and (b) reverse salt flux, J_s of the CTA and modified membranes. DI water and 1.0 M NaCl solution were used as the feed solution and raw solution, respectively.

slightly lower than 11.4 LMH during DI water test. It meant that the modified membrane possessed ideal antifouling ability to biopolymers which were attributed to the hydrophilicity improvement induced by the GO nanosheets [44]. In addition, the decline of surface roughness caused by GO addition can reduce the attachment of biofoulants [45]. Noteworthy, the water flux with SA solution as FS remained constant during the separation. It can be concluded that the influence of reverse salt leakage on the osmosis pressure difference between the draw and FS was inevitable in a short term when 1.0 M NaCl solution was used as DS.

To substantiate the universality of GO-modified membrane antifouling capability to oil foulants, model foulants of different carbon numbers were selected to prepare emulsions. Fig. 8 shows the FO flux behavior in the AL-FS orientation. It was clear that the decline of the water flux due to the reverse salt leakage was observed in baseline at high salinity of DS (4.0 M). Compared with the CTA membrane, the CTA-1%GO membrane was subjected more remarkable flux decline for the higher reverse salt flux. CTA membrane between the baseline and the fouling curve reached 3.9 LMH,

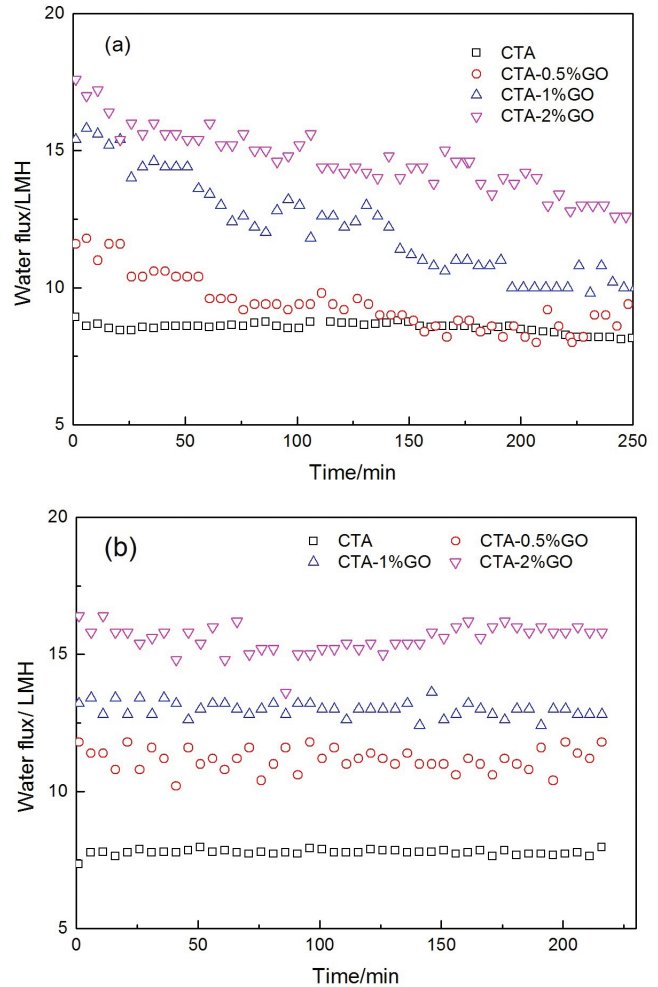


Fig. 7. Flux as a function of the time during the model foulant solution filtration (a) BSA and (b) SA. Model foulant solution with 200 mg L⁻¹ and 1.0 M NaCl solution were used as the feed solution and raw solution under AL-FS mode, respectively.

as shown in Fig. 8(a). Meanwhile, the flux difference of CTA-1%GO membrane was as low as 2.7 LMH. Apparently, GO-modified membrane presented an advantage on water permeability in emulsion separation. From Fig. 8(b), there was no obvious correlation between carbon number of oil molecule and fouling tendency as expected. The excellent antifouling capability of GO-modified CTA membrane under various oil emulsions can be mainly attributed to its superior surface hydrophilicity [46].

It was worthy to point out that the flux decline for BSA solution was more significant than that of SA solution. Such phenomenon could be explained by the influence of ionic strength in FS. As the ionic strength increases, the compression of the electric double layer due to charge screening reduces the electrostatic repulsion among BSA molecules and between the BSA molecules and the membrane [47]. During

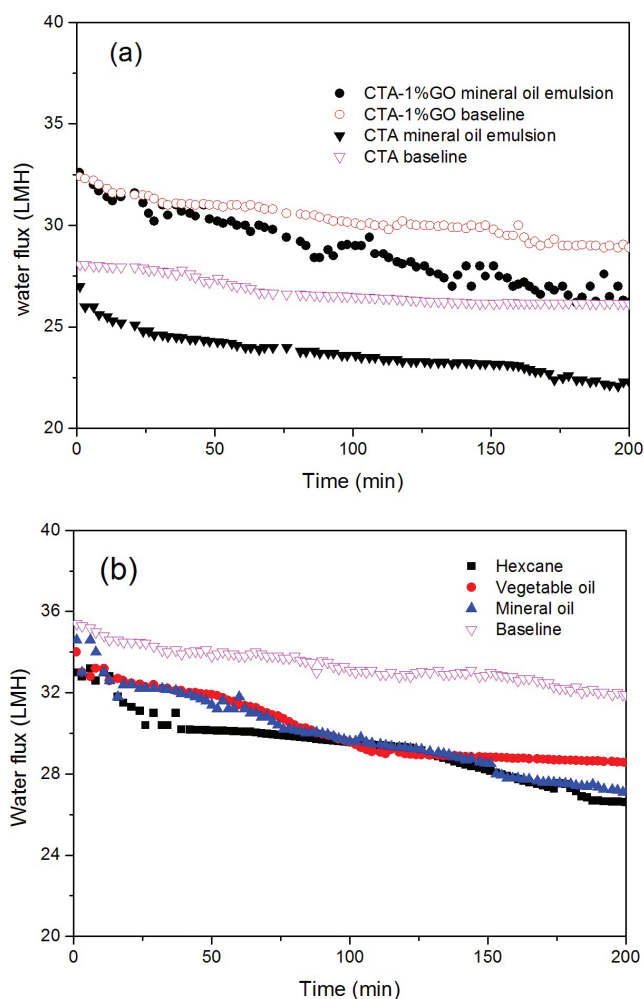


Fig. 8. Flux as a function of the time (a) with CTA and CTA-1%GO membrane during the mineral oil emulsion filtration, (b) with CTA-1%GO membrane during various emulsion filtration. Oil emulsion with 15,000 mg L⁻¹ concentration and 4.0 M NaCl solution were used as the feed solution and raw solution under AL-FS mode, respectively.

the test, the sodium ions continuously diffused from the active surface to the bulk solution due to the reverse salt leakage. As the GO nanosheets embedded in membrane surface were negatively charged, the enrichment of sodium ion occurred due to the electrostatic attraction between GO nanosheets and sodium ions [48], as illustrated in Fig. 9. As a result, there is an increase in the deposition of the BSA molecules on the membrane surface and in the hydraulic resistance of the fouled membrane. As for the SA molecule, it contains sodium ions originally. Thus, the ionic strength did not affect the SA molecule deposition as significantly as BSA molecule. Furthermore, because these anchored oxygenic functional groups have better repulsion for oil colloidal particle [49], the GO-modified membrane presented an ideal performance in oil emulsion separation.

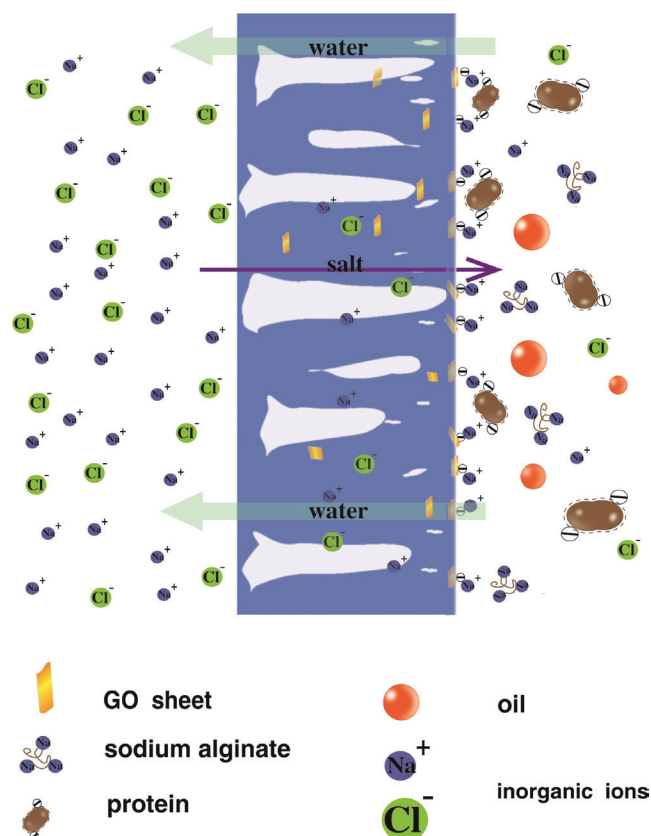


Fig. 9. Illustration of the antifouling mechanisms of GO-modified CTA FO membrane.

4. Conclusions

In this work, the GO-modified FO membranes were prepared by incorporating GO nanosheets in the CTA matrix. The prepared membranes were characterized in terms of morphology and chemical analysis and tested by antifouling experiment using biopolymer foulants and oil emulsion. From the chemical analysis, the hydrogen bonding interactions between the acetyl groups of CTA and the functional groups of the GO nanosheets maybe occurred during the GO-modified CTA membrane preparation. Due to the affinity of GO nanosheets toward water, the nanosheets moved toward top layer and enriched the nanoparticle concentration on membrane surface during the phase inversion. Consequently, the permeability and selectivity of active layer were affected by the concentration of GO in CTA matrix. The change in the water and reverse salt permeability of modified membrane implied that defects in active layer which were possibly induced by the GO clusters emerged on the top surface.

To study GO-modified membrane antifouling ability to biopolymers, BSA and SA were used to simulate the model foulants. The GO-modified membranes were confirmed to possess ideal antifouling ability to biopolymers which were attributed to the hydrophilicity improvement induced by GO nanosheets. However, the increase of ionic strength caused by reverse salt

leakage affects the BSA fouling more significantly than SA fouling. The GO-modified membrane also presented an ideal performance in oil emulsion separation due to its high hydrophilicity.

Acknowledgment

This work is supported by the National Natural Science Foundation of China (Grant No. 51478099, 21477018, 51508082) and National Natural Science Foundation of Shanghai (Grant No. 16ZR1402000).

References

- [1] M.A. Shannon, P.W. Bohn, M. Elimelech, J.G. Georgiadis, B.J. Marinas, A.M. Mayes, Science and technology for water purification in the coming decades, *Nature*, 452 (2008) 301–310.
- [2] T.S. Chung, L. Luo, C.F. Wan, Y. Cui, G. Amy, What is next for forward osmosis (FO) and pressure retarded osmosis (PRO), *Sep. Sci. Technol.*, 156 (2015) 856–860.
- [3] M.A. Darwish, H.K. Abdulrahim, A.S. Hassan, A.A. Mabrouk, A.O. Sharif, The forward osmosis and desalination, *Desalin. Water Treat.*, 57 (2016) 4269–4295.
- [4] B. Van der Bruggen, P. Luis, Forward osmosis: understanding the hype, *Rev. Chem. Eng.*, 31 (2015) 1–12.
- [5] X. Song, Z. Liu, D.D. Sun, Nano gives the answer: breaking the bottleneck of internal concentration polarization with a nanofiber composite forward osmosis membrane for a high water production rate, *Adv. Mater.*, 23 (2011) 3256–3260.
- [6] G.D. Vilakati, M.C.Y. Wong, E.M.V. Hoek, B.B. Mamba, Relating thin film composite membrane performance to support membrane morphology fabricated using lignin additive, *J. Membr. Sci.*, 469 (2014) 216–224.
- [7] M. Tian, C. Qiu, Y. Liao, S. Chou, R. Wang, Preparation of polyamide thin film composite forward osmosis membranes using electrospun polyvinylidene fluoride (PVDF) nanofibers as substrates, *Sep. Sci. Technol.*, 118 (2013) 727–736.
- [8] G. Li, X.M. Li, T. He, B. Jiang, C. Gao, Cellulose triacetate forward osmosis membranes: preparation and characterization, *Desal. Water Treat.*, 51 (2013) 2656–2665.
- [9] P.G. Ingole, W. Choi, K.H. Kim, H.D. Jo, W.K. Choi, J.S. Park, H.K. Lee, Preparation, characterization and performance evaluations of thin film composite hollow fiber membrane for energy generation, *Desalination*, 345 (2014) 136–145.
- [10] C.Y.Y. Tang, Q.H. She, W.C.L. Lay, R. Wang, R. Field, A.G. Fane, Modeling double-skinned FO membranes, *Desalination*, 283 (2011) 178–186.
- [11] S. Zhang, K.Y. Wang, T.S. Chung, H. Chen, Y. Jean, G. Amy, Well-constructed cellulose acetate membranes for forward osmosis: minimized internal concentration polarization with an ultra-thin selective layer, *J. Membr. Sci.*, 360 (2010) 522–535.
- [12] J. Su, T.S. Chung, Sublayer structure and reflection coefficient and their effects on concentration polarization and membrane performance in FO processes, *J. Membr. Sci.*, 376 (2011) 214–224.
- [13] Z.P. Smith, B.D. Freeman, Graphene oxide: a new platform for high-performance gas- and liquid-separation membranes, *Angew. Chem. Int. Ed.*, 53 (2014) 10286–10288.
- [14] Z. Jia, Y. Wang, Covalently crosslinked graphene oxide membranes by esterification reactions for ions separation, *J. Mater. Chem. A*, 3 (2015) 4405–4412.
- [15] H. Huang, Y. Ying, X. Peng, Graphene oxide nanosheet: an emerging star material for novel separation membranes, *J. Mater. Chem. A*, 2 (2014) 13772–13782.
- [16] S.G. Kim, D.H. Hyeon, J.H. Chun, B.H. Chun, S.H. Kim, Novel thin nanocomposite RO membranes for chlorine resistance, *Desal. Water Treat.*, 51 (2013) 6338–6345.
- [17] J. Lee, H.R. Chae, Y.J. Won, K. Lee, C.H. Lee, H.H. Lee, I.C. Kim, J.M. Lee, Graphene oxide nanoplatelets composite membrane with hydrophilic and antifouling properties for wastewater treatment, *J. Membr. Sci.*, 448 (2013) 223–230.
- [18] J. Zhang, Z. Xu, W. Mai, C. Min, B. Zhou, M. Shan, Y. Li, C. Yang, Z. Wang, X. Qian, Improved hydrophilicity, permeability, antifouling and mechanical performance of PVDF composite ultrafiltration membranes tailored by oxidized low-dimensional carbon nanomaterials, *J. Mater. Chem. A*, 1 (2013) 3101–3111.
- [19] M. Ionita, E. Vasile, L.E. Crica, S.I. Voicu, A.M. Pandele, S. Dinescu, L. Predoiu, B. Galateanu, A. Hermenean, M. Costache, Synthesis, characterization and in vitro studies of polysulfone/graphene oxide composite membranes, *Composites Part B*, 72 (2015) 108–115.
- [20] H.M. Hegab, A. ElMekawy, T.G. Barclay, A. Michelmore, L. Zou, C.P. Saint, M. Ginic-Markovic, Fine-tuning the surface of forward osmosis membranes via grafting graphene oxide: performance patterns and biofouling propensity, *ACS App. Mater. Interface.*, 7 (2015) 18004–18016.
- [21] Y.P. Tang, J.X. Chan, T.S. Chung, M. Weber, C. Staudt, C. Maletzko, Simultaneously covalent and ionic bridging towards antifouling of GO-embedded nanocomposite hollow fiber membranes, *J. Mater. Chem. A*, 3 (2015) 10573–10584.
- [22] D.C. Marcano, D.V. Kosynkin, J.M. Berlin, A. Sinitskii, Z. Sun, A. Slesarev, L.B. Alemany, W. Lu, J.M. Tour, Improved synthesis of graphene oxide, *ACS Nano*, 4 (2010) 4806–4814.
- [23] R.C. Ong, T.S. Chung, Fabrication and positron annihilation spectroscopy (PAS) characterization of cellulose triacetate membranes for forward osmosis, *J. Membr. Sci.*, 394 (2012) 230–240.
- [24] W. Pusch, R. Riley, Relation between salt rejection r and reflection coefficient σ of asymmetric cellulose acetate membranes, *Desalination*, 14 (1974) 389–393.
- [25] S. Loeb, L. Titelman, E. Korngold, J. Freiman, Effect of porous support fabric on osmosis through a Loeb-Sourirajan type asymmetric membrane, *J. Membr. Sci.*, 129 (1997) 243–249.
- [26] L. Yu, Y. Zhang, B. Zhang, J. Liu, H. Zhang, C. Song, Preparation and characterization of HPEI-GO/PES ultrafiltration membrane with antifouling and antibacterial properties, *J. Membr. Sci.*, 447 (2013) 452–462.
- [27] M.J. Park, S. Phuntsho, T. He, G.M. Nisola, L.D. Tijing, X.M. Li, G. Chen, W.J. Chung, H.K. Shon, Graphene oxide incorporated polysulfone substrate for the fabrication of flat-sheet thin-film composite forward osmosis membranes, *J. Membr. Sci.*, 493 (2015) 496–507.
- [28] H. Wu, B. Tang, P. Wu, Development of novel SiO₂-GO nano-hybrid/polysulfone membrane with enhanced performance, *J. Membr. Sci.*, 451 (2014) 94–102.
- [29] Y. Wang, R. Ou, H. Wang, T. Xu, Graphene oxide modified graphitic carbon nitride as a modifier for thin film composite forward osmosis membrane, *J. Membr. Sci.*, 475 (2015) 281–289.
- [30] R. Abedini, S.M. Mousavi, R. Aminzadeh, A novel cellulose acetate (CA) membrane using TiO₂ nanoparticles: Preparation, characterization and permeation study, *Desalination*, 277 (2011) 40–45.
- [31] M. Ionita, E. Vasile, L.E. Crica, S.I. Voicu, A.M. Pandele, S. Dinescu, L. Predoiu, B. Galateanu, A. Hermenean, M. Costache, Synthesis, characterization and in vitro studies of polysulfone/graphene oxide composite membranes, *Composites Part B*, 72 (2015) 108–115.
- [32] O. Arous, H. Kerdjoudj, P. Seta, Comparison of carrier-facilitated silver (i) and copper (ii) ions transport mechanisms in a supported liquid membrane and in a plasticized cellulose triacetate membrane, *J. Membr. Sci.*, 241 (2004) 177–185.
- [33] M. Amini, A. Rahimpour, M. Jahanshahi, Forward osmosis application of modified TiO₂-polyamide thin film nanocomposite membranes, *Desal. Water Treat.*, 57 (2016) 14013–14023.
- [34] N. Misdan, A.F. Ismail, N. Hilal, Recent advances in the development of (bio)fouling resistant thin film composite membranes for desalination, *Desalination*, 380 (2016) 105–111.
- [35] A. Zirehpour, A. Rahimpour, F. Seyyedpour, M. Jahanshahi, Developing new CTA/CA-based membrane containing hydrophilic nanoparticles to enhance the forward osmosis desalination, *Desalination*, 371 (2015) 46–57.
- [36] M. Wada, R. Hori, X-Ray Diffraction Study of the Thermal Expansion Behavior of Cellulose Triacetate I, *J. Polym. Sci. B*, 47 (2009) 517–523.

- [37] D. Galpaya, M. Wang, M. Liu, N. Motta, E. Waclawik, C. Yan, Recent advances in fabrication and characterization of graphene-polymer nanocomposites, *Graphene*, 1 (2012) 30–49.
- [38] T.S. Chung, L.Y. Jiang, Y. Li, S. Kulprathipanja, Mixed matrix membranes (MMMs) comprising organic polymers with dispersed inorganic fillers for gas separation, *Prog. Polym. Sci.*, 32 (2007) 483–507.
- [39] L.A. Hoover, J.D. Schiffman, M. Elimelech, Nanofibers in thin-film composite membrane support layers: Enabling expanded application of forward and pressure retarded osmosis, *Desalination*, 308 (2013) 73–81.
- [40] W.C.L. Lay, J. Zhang, C. Tang, R. Wang, Y. Liu, A.G. Fane, Analysis of Salt Accumulation in a Forward Osmosis System, *Sep. Sci. Technol.*, 47 (2012) 1837–1848.
- [41] W. Gao, H. Liang, J. Ma, M. Han, Z.I. Chen, Z.S. Han, G.B. Li, Membrane fouling control in ultrafiltration technology for drinking water production: A review, *Desalination*, 272 (2011) 1–8.
- [42] T.Y. Cath, M. Elimelech, J.R. McCutcheon, R.L. McGinnis, A. Achilli, D. Anastasio, A.R. Brady, et al., Standard methodology for evaluating membrane performance in osmotically driven membrane processes, *Desalination*, 312 (2013) 31–38.
- [43] X. Wang, B. Yuan, Y. Chen, X. Li, Y. Ren, Integration of micro-filtration into osmotic membrane bioreactors to prevent salinity build-up, *Bioresour. Technol.*, 167 (2014) 116–123.
- [44] W.K. Zhu, H.P. Cong, H.B. Yao, L.B. Mao, A.M. Asiri, K.A. Alamry, H.M. Marwani, S.H. Yu, Bioinspired, ultrastrong, highly biocompatible, and bioactive natural polymer/graphene oxide nanocomposite films, *Small*, 11 (2015) 4298–4302.
- [45] W. Luo, F.I. Hai, W.E. Price, L.D. Nghiem, Water extraction from mixed liquor of an aerobic bioreactor by forward osmosis: Membrane fouling and biomass characteristics assessment, *Sep. Sci. Technol.*, 145 (2015) 56–62.
- [46] D.D. Kaombe, M.B. Hagg, Forward osmosis for the dewatering of pyrolysis oil aqueous phase, *Sep. Sci. Technol.*, 138 (2014) 92–97.
- [47] P. Zhao, B. Gao, Q. Yue, H.K. Shon, Q. Li, Fouling of forward osmosis membrane by protein (BSA): effects of pH, calcium, ionic strength, initial permeate flux, membrane orientation and foulant composition, *Desal. Water Treat.*, 57 (2016) 13415–13424.
- [48] L. Wang, N. Wang, J. Li, J. Li, W. Bian, S. Ji, Layer-by-layer self-assembly of polycation/GO nanofiltration membrane with enhanced stability and fouling resistance, *Sep. Sci. Technol.*, 160 (2016) 123–131.
- [49] D. Qin, Z. Liu, D.D. Sun, X. Song, H. Bai, A new nanocomposite forward osmosis membrane custom-designed for treating shale gas wastewater, *Sci. Rep.-UK*, 5 (2015) 1–13.